

Electronic Supplementary Information

Nickel Metal-Organic Framework Implanted on Graphene and Incubated to be Ultrasmall Nickel Phosphide Nanocrystals as Highly Efficient Water Splitting Electrocatalyst

Liting Yan,^a Huimin Jiang,^a Yanlong Xing,^{b,*} Ying Wang,^a Dandan Liu,^a Xin Gu,^a

Pengcheng Dai,^a Liangjun Li,^a Xuebo Zhao^{a,*}

^a Research Centre of New Energy Science and Technology, Research Institute of
Unconventional Oil & Gas and Renewable Energy, China University of Petroleum
(East China), Qingdao 266580, P. R. China. *E-mail: zhaoxuebo@upc.edu.cn

^b Leibniz Institute for Analytical Sciences, Berlin 12489, Germany.

*E-mail: yanlong.xing@isas.de

I. Materials

II. Additional Methods

III. Supplementary Figures and Tables

Fig. S1. PXRD patterns of MOF-74-Ni and MOF-74-Ni/GO.

Fig. S2. PXRD patterns of Ni₂P/C and Ni₂P particles.

Fig. S3. SEM images of MOF-74-Ni and MOF-74-Ni/GO.

Fig. S4. XPS survey spectra of the Ni₂P/rGO.

Fig.S5. Comparison of highresolution XPS spectra in the C 1s region of MOF-74-Ni/GO and Ni₂P/rGO.

Fig. S6. SEM images of the exposed defects of rGO sheets on the Ni₂P/rGO.

Fig. S7. Elemental mappings of the Ni₂P/rGO.

Fig. S8. TEM images of MOF-74-Ni/GO.

Fig. S9. Raman spectra of Ni₂P/rGO and Ni₂P/C.

Fig. S10. Electrochemical cyclic voltammetry curves of Ni₂P particles, Ni₂P/C, and Ni₂P/rGO at different potential scanning rates.

Fig. S11. N₂ adsorption–desorption isotherm of Ni₂P particles, Ni₂P/C, and Ni₂P/rGO.

Fig. S12. LSV of Ni₂P/rGO before and after the pre-activation process.

Fig. S13. Highresolution XPS spectra in the Ni 2p region of Ni₂P/rGO after the pre-activation process.

Fig. S14. TEM images of Ni₂P/rGO after the pre-activation process.

Fig. S15. HRTEM images of Ni₂P/rGO after the pre-activation process.

Fig. S16. PXRD patterns of Ni₂P/rGO after the pre-activation process.

Fig. S17. Highresolution XPS spectra in the Ni 2p region of Ni₂P/rGO after the continuous CV cycles.

Fig. S18. Electrocatalytic performance of Ni₂P/rGO in different electrolyte.

Fig. S19. LSV of Ni₂P/rGO/NF for a) OER and b) HER.

Fig. S20. OER polarization curves catalyzed by Ni₂P/rGO/NF with different mass loading.

Fig. S21. a) The overall water splitting performance and catalytic stability of Ni₂P/rGO and Pt/C-RuO₂ couple.

Table S1. Summary of ICP results of as-prepared catalysts..

Table S2. Summary of various TMPs catalysts for OER.

Table S3. Summary of various TMPs catalysts for HER.

Table S4. Summary of various catalytic electrodes for overall water splitting.

I. Materials:

Nickel acetate tetrahydrate ($\text{Ni}(\text{Ac})_2 \cdot 4\text{H}_2\text{O}$, 98 wt%), ethanol (≥ 99.7 wt%), potassium hydroxide (KOH, ≥ 85.0 wt%) and sodium hydroxide (NaOH, ≥ 96 wt%) were purchased from Sinopharm Chemical Reagent Co. Ltd. (SCRC). 2,5-dihydroxyterephthalic acid (DHTA, 98 wt%) was obtained from Chemsoon Co. Ltd.. Sodium hypophosphite ($\text{NaH}_2\text{PO}_2 \cdot \text{H}_2\text{O}$, 99 wt%) and ruthenium(IV) oxide (RuO_2) were purchased from Aladdin. Graphene oxide (GO) aqueous solution, nickel foam (NF) and carbon rod were purchased from Shandong Haike Chemical Group Co.,. Nafion solution (5 wt% in a mixture of lower aliphatic alcohols and water) and platinum on carbon (Pt/C, 10 wt %) were purchased from Sigma-Aldrich Co. LLC.. All reagents were used without further purification.

II. Additional Methods:

2.1 Estimation of Effective Electrochemical Active Surface Area (ECSA).¹⁻³

The ECSA was determined from the double layer capacitance (C_{dl}) of the catalyst surface. The C_{dl} was determined by measuring cyclic voltammograms (CVs) with multiple scan rates in nonfaradaic potential region. In this potential region, all measured currents are assumed to be associated with double-layer charging. The potential range typically centered at the open circuit potential (OCP) with a potential window of 0.1 V. In this work, CVs were measured in a potential range of 1.30-1.40 V vs. RHE at different scan rates. The ECSA of a catalyst is calculated by dividing the C_{dl} with specific capacitance of the sample according to equation $\text{ECSAs} = C_{dl}/C_s$, where C_s is the specific capacitance of the sample or the capacitance of an atomically smooth planar

surface of the material per unit area under identical electrolyte conditions. For the estimates of surface area, we use general specific capacitances of $C_s = 0.85 \text{ mF/cm}^2$ in 1.0 M KOH.

2.2 Calculation of turnover frequency (TOF).¹⁻³

Details concerning the calculation of TOF are shown as below. The values of TOF are calculated assuming that all Ni ions in the catalysts are active and contribute to the catalytic reaction (the lowest TOF values were calculated)

$$\text{TOF} = jS/(4Fn)$$

Here, j (A/cm^2) is the measured current density at an overpotential of 300 mV; S (0.071 cm^2) is the surface area of GCE; the number of 4 means 4 electrons transfer in OER; F is Faraday constant ($96485.3 \text{ C mol}^{-1}$), and n is the Ni ions molar number calculated from mass loading density (m , 0.25 mg cm^{-2}) and ICP results of catalyst.

2.3 Calculation of specific activity.^{1,3}

The values of specific activity (mA cm^{-2}) are calculated from the BET surface area S_{BET} ($\text{m}^2 \text{ g}^{-1}$), the catalyst loading density m ($0.5, 1.0, 2.0, 4.0, 8.0 \text{ mg cm}^{-2}$), and the measured current density j (mA cm^{-2}) at the overpotential of 300 mV

$$\text{Specific activity} = j/10S_{\text{BET}}m$$

III. Supplementary Figures and Tables

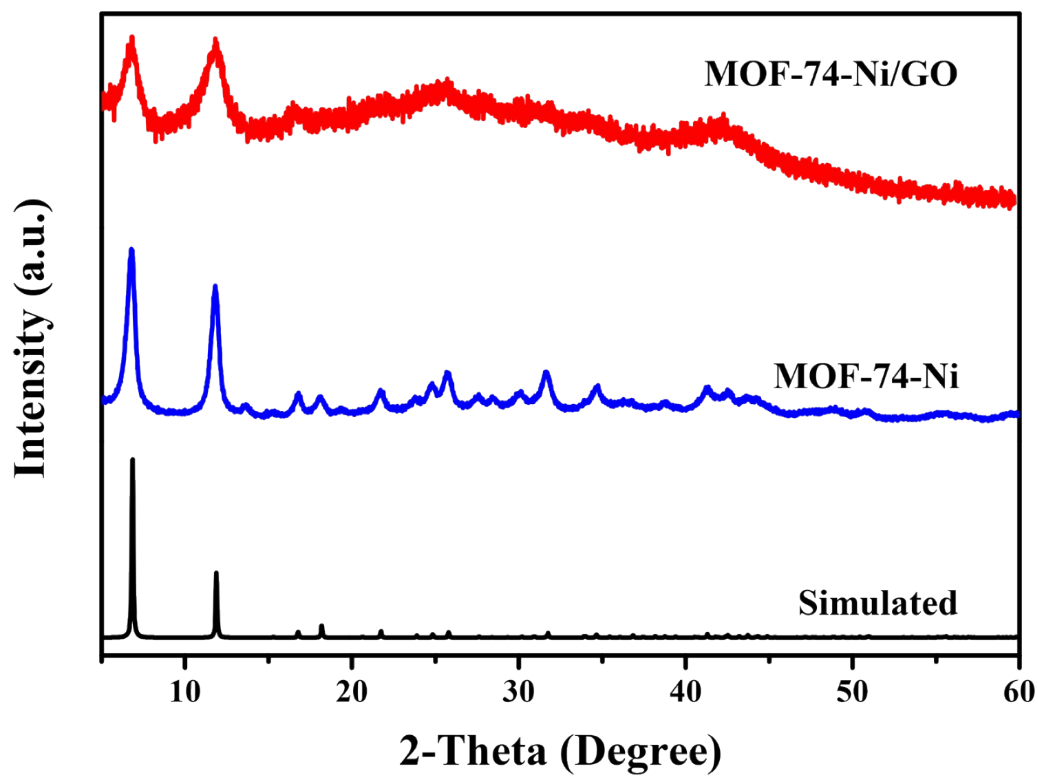


Fig. S1. PXRD patterns of MOF-74-Ni and MOF-74-Ni/GO.

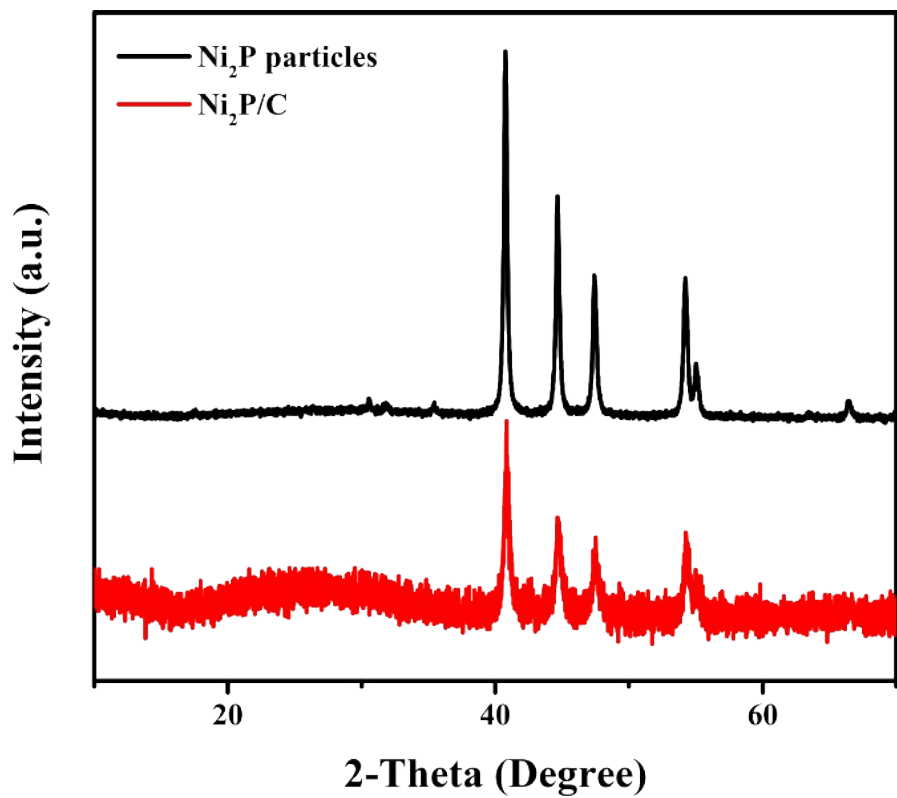


Fig. S2. PXRD patterns of Ni₂P/C and Ni₂P particles.

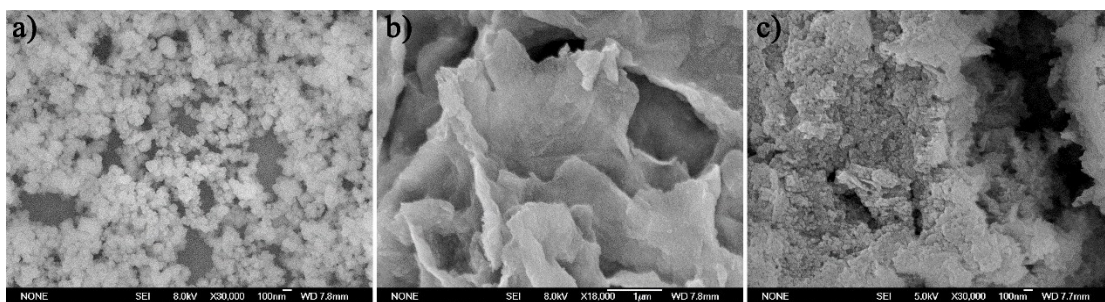


Fig. S3. Low magnification SEM images of a)MOF-74-Ni and b)MOF-74-Ni/GO, and c) high magnification SEM images of MOF-74-Ni/GO.

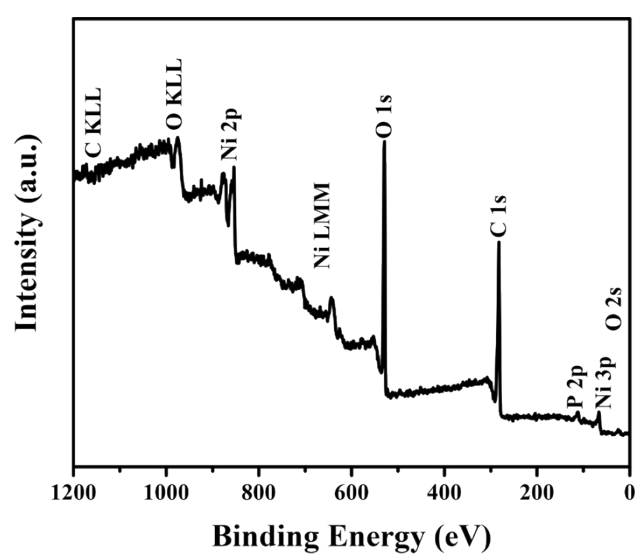


Fig. S4. XPS survey spectra of the Ni₂P/rGO.

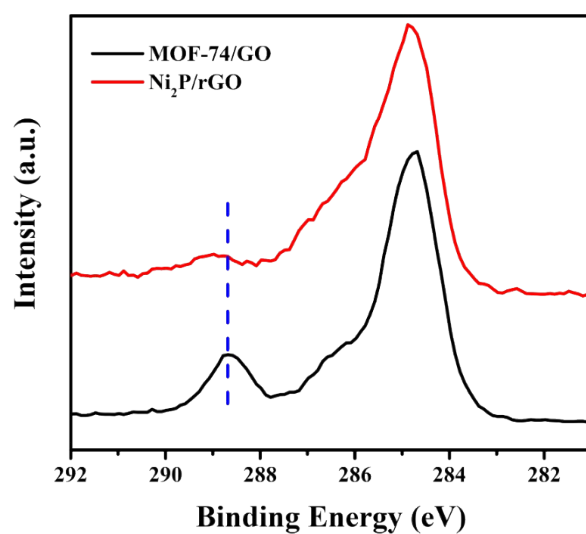


Fig. S5. Comparison of high-resolution XPS spectra in the C 1s region of MOF-74-Ni/GO and Ni₂P/rGO.

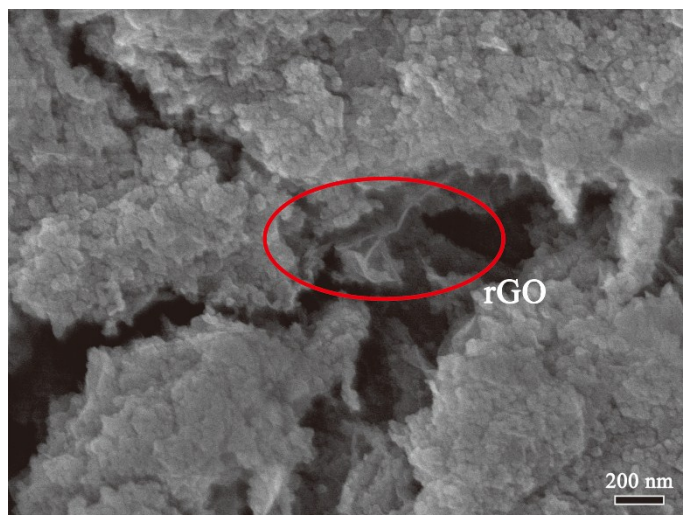


Fig. S6. SEM images of the exposed defects of rGO sheets on the Ni₂P/rGO.

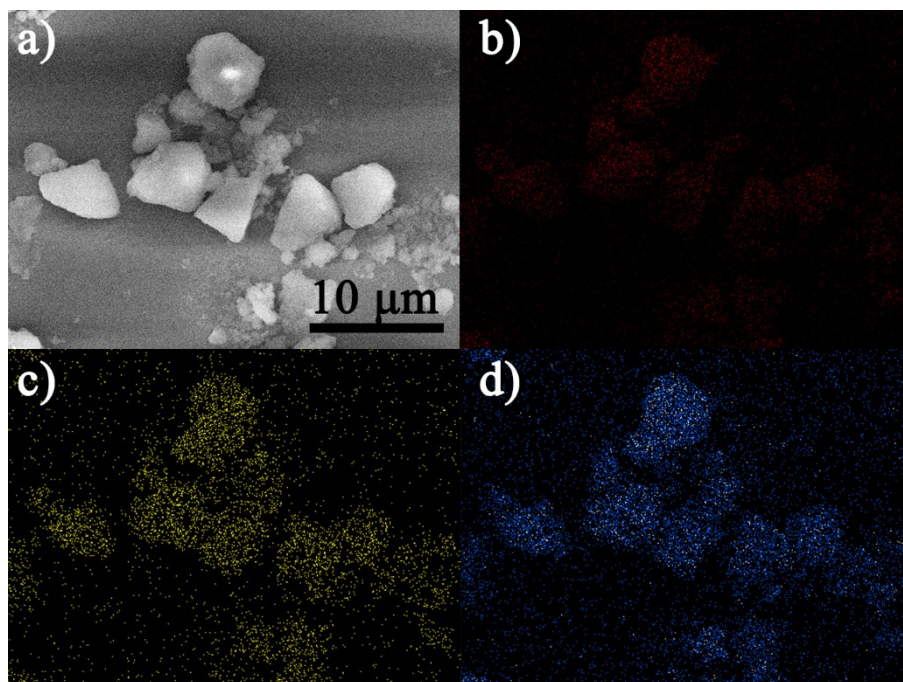


Fig. S7. Elemental mappings of the Ni₂P/rGO. a) Low magnification SEM images of the Ni₂P/rGO, b) C, c) Ni, and d) P.

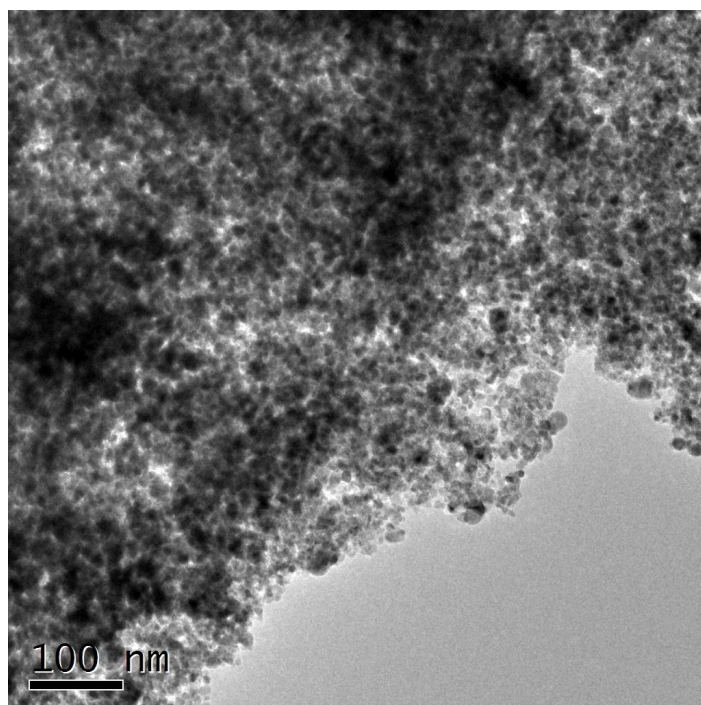


Fig. S8. TEM images of MOF-74-Ni/GO.

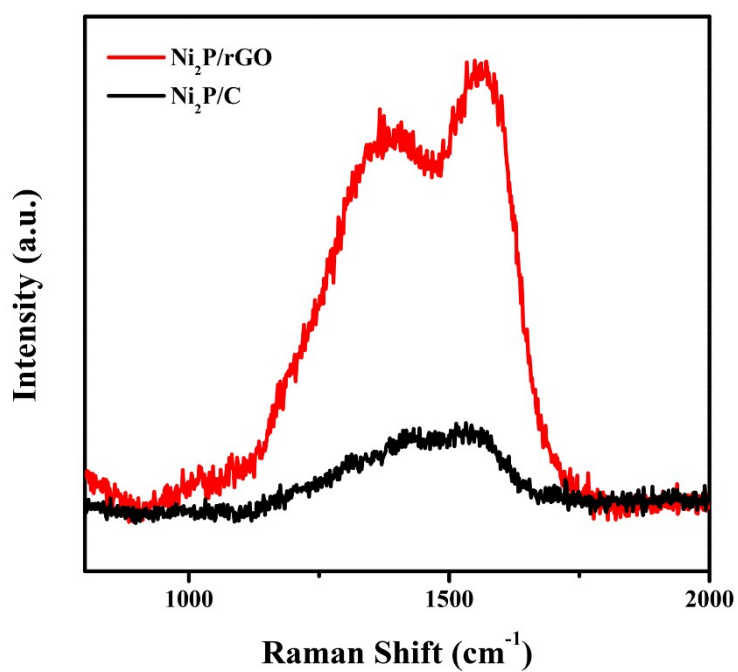


Fig. S9. Raman spectra of Ni₂P/rGO and Ni₂P/C.

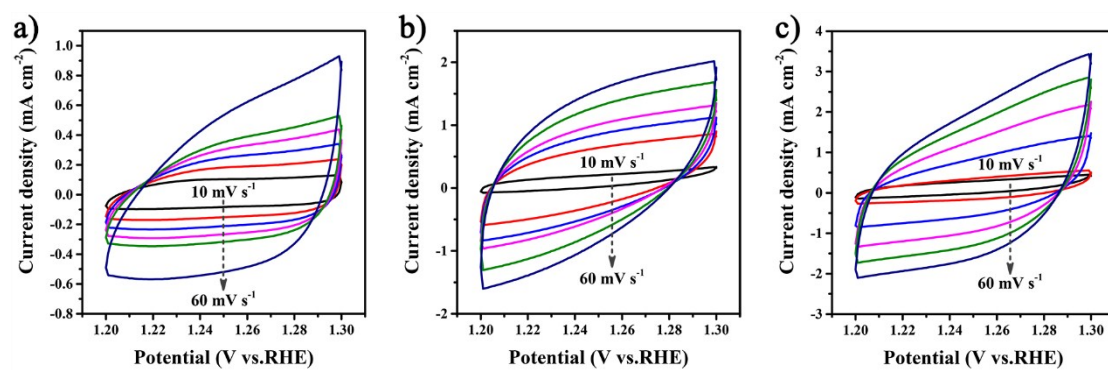


Fig. S10. Electrochemical cyclic voltammetry curves of a) Ni₂P particles, b) Ni₂P/C, and c) Ni₂P/rGO at different potential scanning rates.

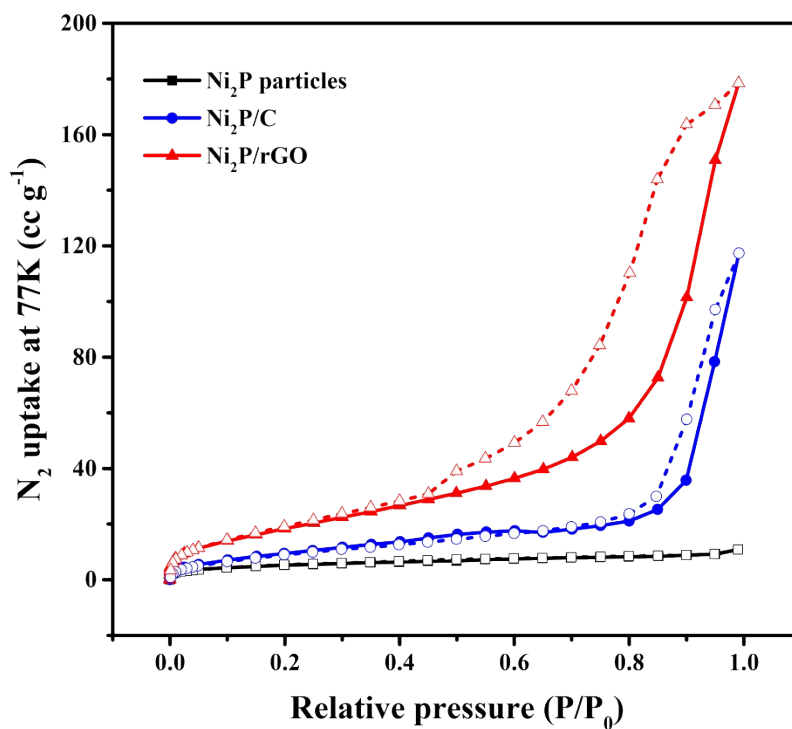


Fig. S11. N₂ adsorption–desorption isotherm of Ni₂P particles, Ni₂P/C, and Ni₂P/rGO.

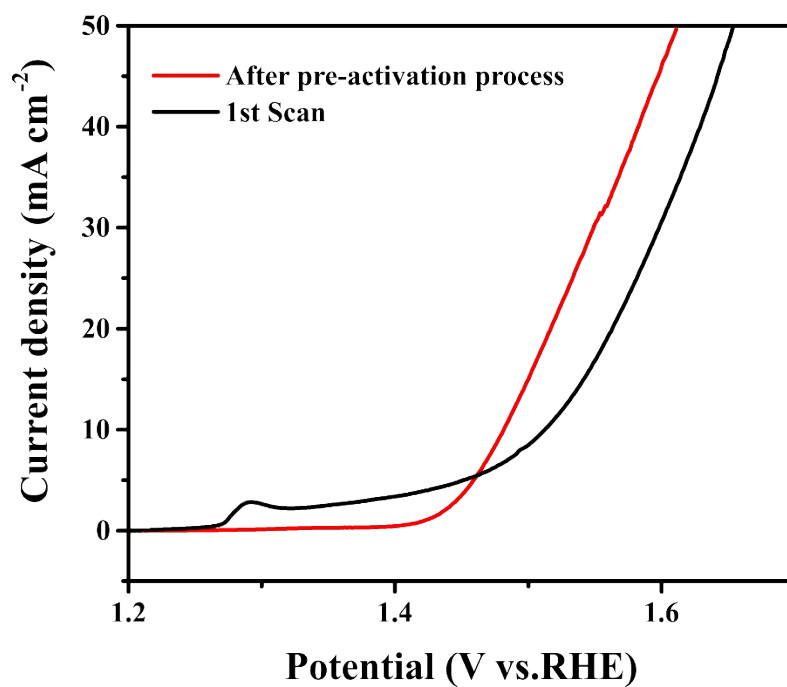


Fig. S12. LSV of Ni₂P/rGO before and after the pre-activation process.

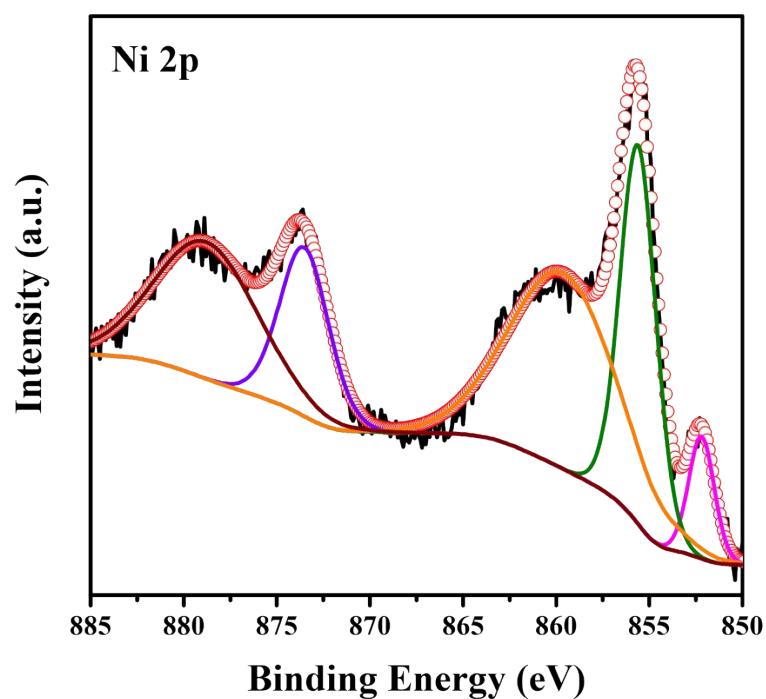


Fig. S13. High-resolution XPS spectra in the Ni 2p region of Ni₂P/rGO after the pre-activation process.

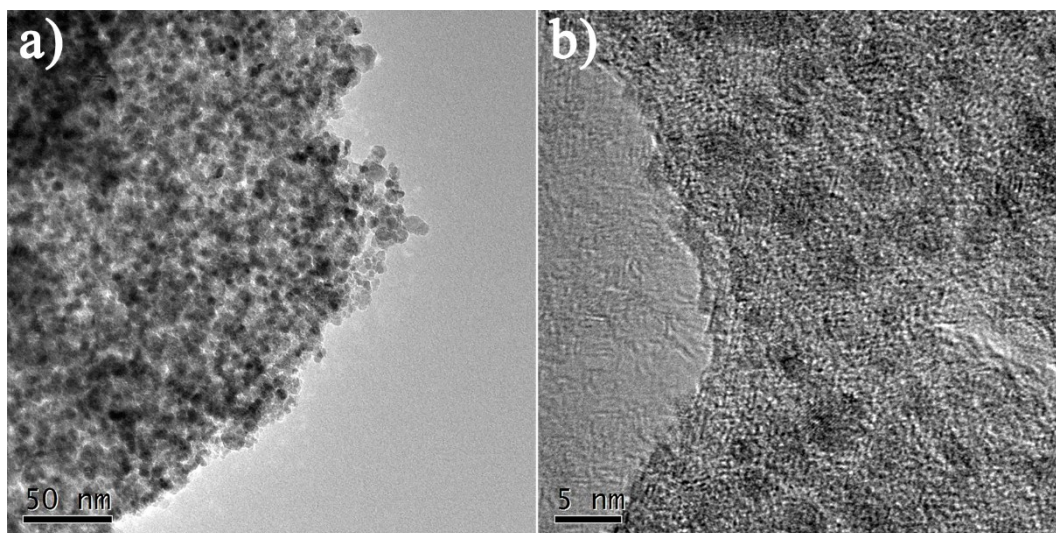


Fig. S14. TEM images of Ni₂P/rGO after the pre-activation process.

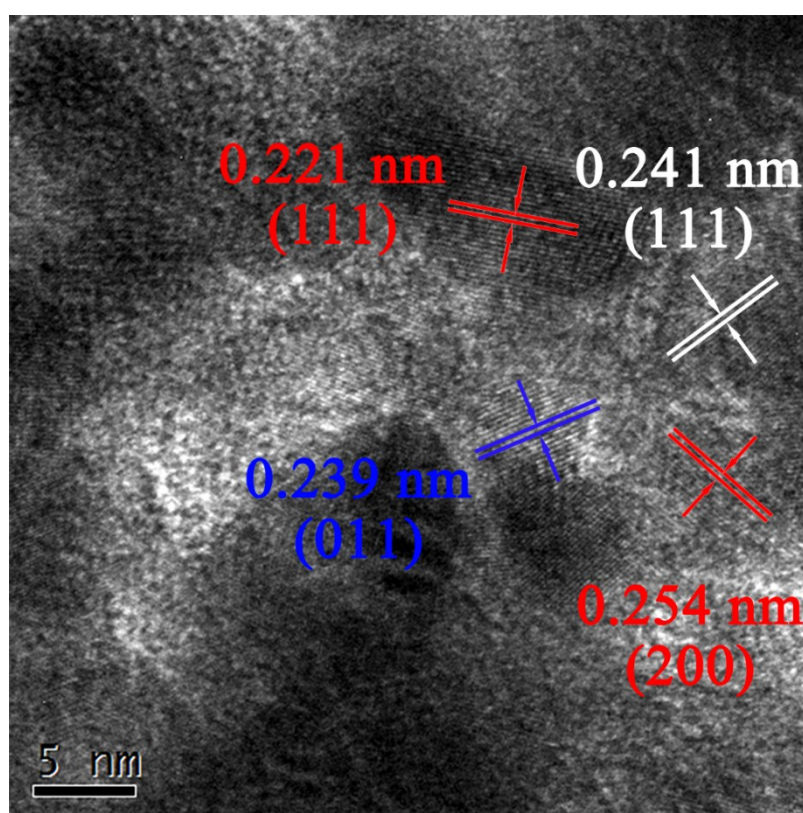


Fig. S15. HRTEM images of Ni₂P/rGO after the pre-activation process.

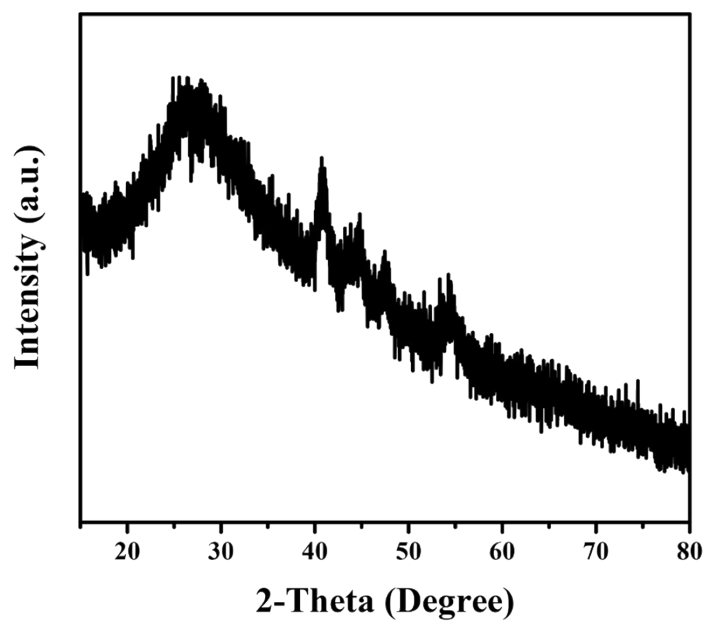


Fig. S16. PXRD patterns of Ni₂P/rGO after the pre-activation process.

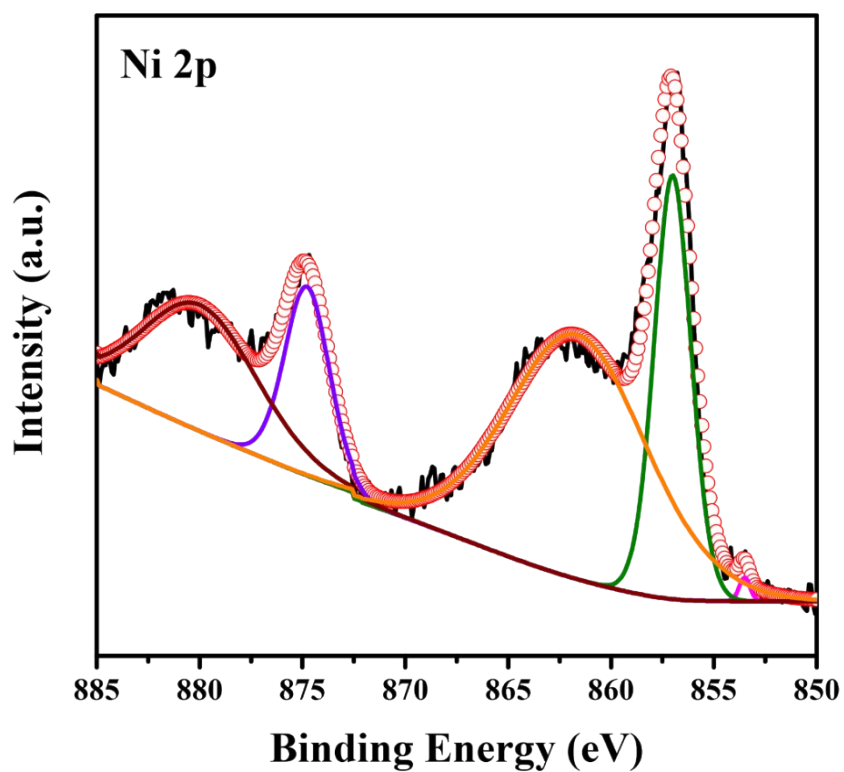


Fig. S17. High-resolution XPS spectra in the Ni 2p region of Ni₂P/rGO after the continuous CV cycles.

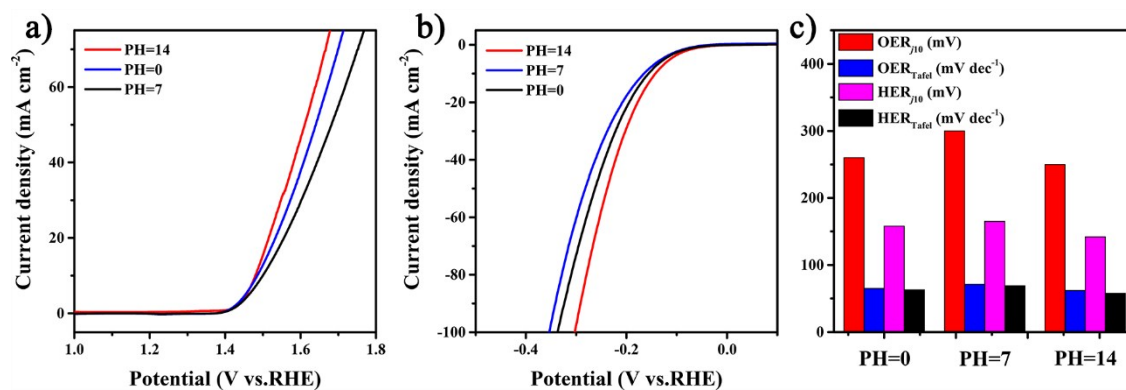


Fig. S18. a) OER polarization curves, b) HER polarization curves, and c) Summary of Tafel slope and overpotential at $j = 10 \text{ mA cm}^{-2}$ for the OER and HER catalyzed by $\text{Ni}_2\text{P/rGO}$ in 1.0 M KOH (pH = 14), 1.0 M PBS (pH = 7), and 0.5 M H_2SO_4 (pH = 0).

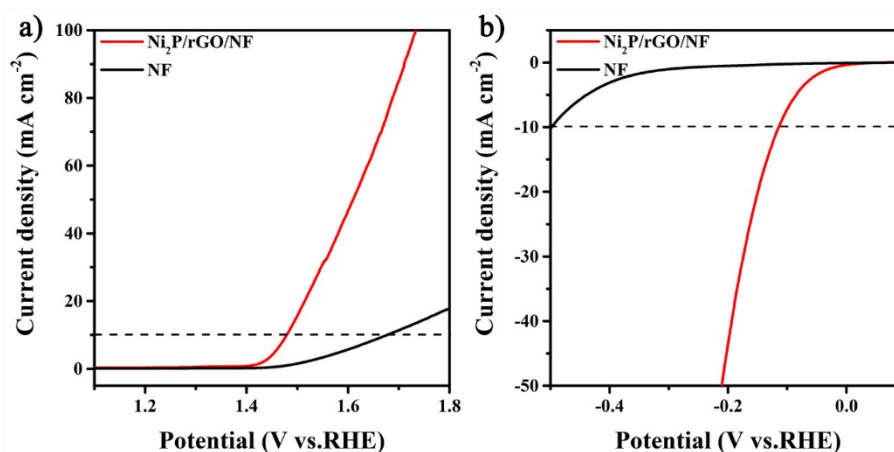


Fig. S19. LSV of $\text{Ni}_2\text{P/rGO/NF}$ for a) OER and b) HER.

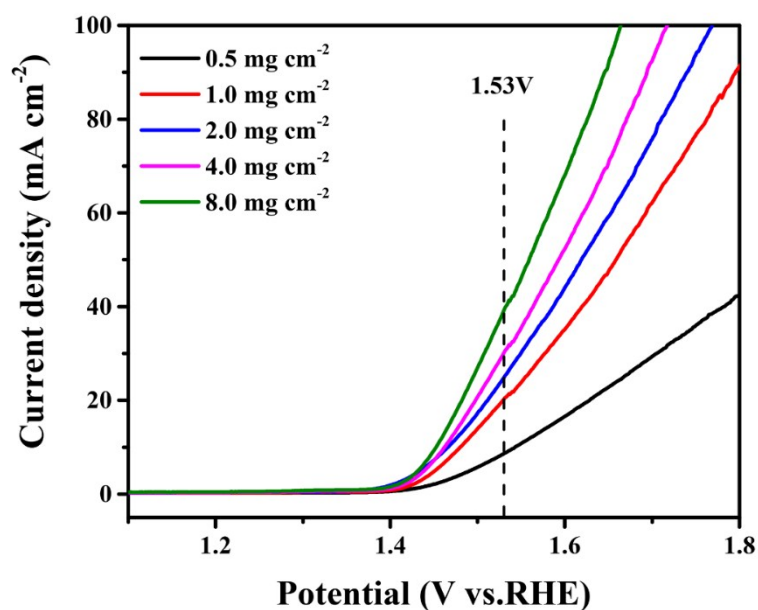


Fig. S20. OER polarization curves catalyzed by $\text{Ni}_2\text{P/rGO/NF}$ with different mass loading.

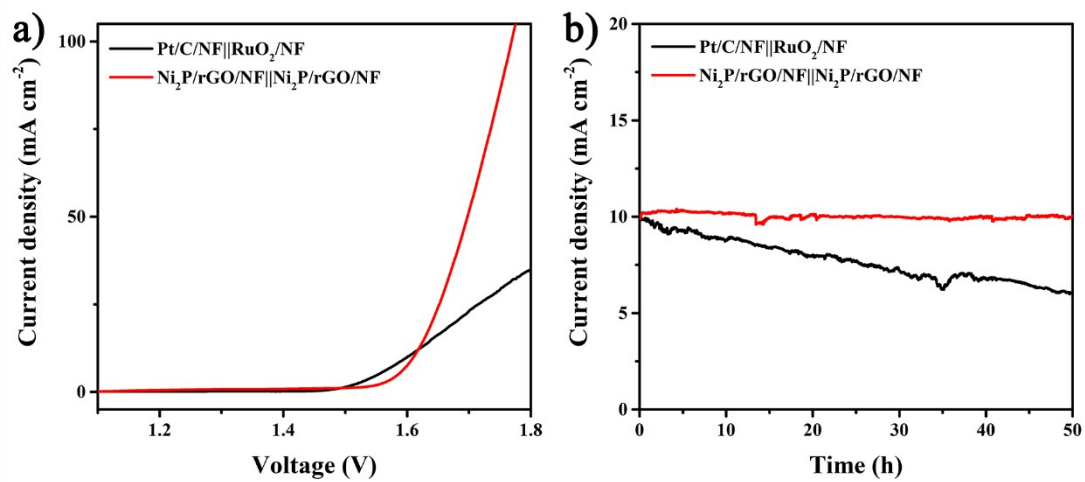


Fig. S21. a) The overall water splitting performance of Ni₂P/rGO and Pt/C-RuO₂ couple. b) The catalytic stability of the Ni₂P/rGO and Pt/C-RuO₂ couple.

Table S1. Summary of ICP results of as-prepared catalysts.

Samples	Ni content/ wt%
Ni ₂ P/rGO	19.8
Ni ₂ P/C	28.5
Ni ₂ P particles	47.6

Table S2. Summary of various TMPs catalysts for OER.

Catalysts	Loading/ mg cm⁻²	Overpotential@ <i>j</i>₁₀ / mV	Electrolyte	Reference
Ni ₂ P/rGO	0.25	260	1.0 M KOH	This work
Ni ₂ P/rGO/NF	1.0	250	1.0 M KOH	This work
Ni _{0.69} Co _{0.31} -P	3.5	266	1.0 M KOH	4
Ni ₂ P nanowires	0.14	290	1.0 M KOH	5
Ni-P	0.20	300	1.0 M KOH	6
Ni ₂ P nanoparticles	0.14	290	1.0 M KOH	7
Ni ₂ P/Ni/NF	—	200	1.0 M KOH	8
Ni ₂ P@C/G	0.25	285	1.0 M KOH	9
Ni ₂ P@C	0.25	340	1.0 M KOH	9
Ni ₂ P/FTO	1.0	330	1.0 M KOH	10
Ni ₁₂ P ₅ /FTO	1.0	295	1.0 M KOH	10
Co ₂ P/CoFoil	—	319	1.0 M KOH	11
CoP hollow polyhedron	0.102	400	1.0 M KOH	12
Co-P/NC	1.0	319	1.0 M KOH	13
Co-Fe-P-1.7	—	260	1.0 M KOH	2
Cu _{0.3} Co _{2.7} P/NC	0.4	190	1.0 M KOH	14
NiCoP/rGO	—	270	1.0 M KOH	15
Ni _{0.51} Co _{0.49} P	—	239	1.0 M KOH	16
NiCoP/Ti	0.75	310	1.0 M KOH	17
NiCoP/NF	—	280	1.0 M KOH	18
Co ₄ Ni ₁ P NTs	0.19	245	1.0 M KOH	1
NiCoP/C nanoboxes	—	330	1 M KOH	19

Table S3. Summary of various TMPs catalysts for HER.

Catalysts	Loading/ mg cm ⁻²	Overpotential@ j_{10} / mV	Electrolyte	Reference
Ni ₂ P/rGO	0.25	142	1.0 M KOH	This work
Ni ₂ P/rGO/NF	0.25	115	1.0 M KOH	This work
Ni _{0.69} Co _{0.31} -P	3.5	167	1.0 M KOH	4
Ni ₂ P/NF	3	85	1.0 M KOH	10
Ni ₁₂ P ₅ /NF	3	170	1.0 M KOH	10
Ni ₂ P nanoparticles	1.8	220	1.0 M KOH	7
Ni ₅ P ₄ on Nickel foil	—	150	1.0 M KOH	20
CoP nanowire	0.92	335	1.0 M KOH	21
CoP/CC	—	209	1.0 M KOH	21
Co ₂ P/Co-Foil	—	154	1.0 M KOH	11
CoP hollow polyhedron	0.102	159	0.5 M H ₂ SO ₄	12
Co-P/NC	1.0	154	1.0 M KOH	13
Co-Fe-P-1.7	—	295	1.0 M KOH	2
Cu _{0.3} Co _{2.7} P/NC	0.4	220	1.0 M KOH	14
NiCoP/rGO	—	209	1.0 M KOH	15
Ni _{0.51} Co _{0.49} P	—	82	1.0 M KOH	16
NiCoP/Ti	0.75	97	0.5 M H ₂ SO ₄	17
NiCoP/NF	—	32	1.0 M KOH	18
Co ₄ Ni ₁ P NTs	0.19	110	1.0 M KOH	1

Table S4. Summary of various catalytic electrodes for overall water splitting.

Catalysts	Voltages@j_{10}/V	Electrolyte	Reference
Ni ₂ P/rGO/NF	1.61	1.0 M KOH	This work
Ni ₂ P nanowires	1.63	1.0 M KOH	5
Ni ₂ P/Ni/NF	1.49	1.0 M KOH	8
Ni ₅ P ₄ films	1.69	1.0 M KOH	20
Ni-P foam	1.64	1.0 M KOH	22
CP@Ni-P	1.63	1.0 M KOH	23
CoP/GO-400	1.7	1.0 M KOH	24
Co-P	1.65	1.0 M KOH	25
Ni _{0.69} Co _{0.31} -P	1.59	1.0 M KOH	4
NiCoP/rGO	1.59	1.0 M KOH	15
Co-Fe-P-1.7	1.60	1.0 M KOH	2
NiCoP/Ti	1.64	1.0 M KOH	17
NiCoP/NF	1.58	1.0 M KOH	18
Co ₄ Ni ₁ P NTs	1.59	1.0 M KOH	1
Ni-Fe-P	1.52	1.0 M KOH	26
NiCo ₂ O ₄	1.65	1.0 M KOH	27
Ni ₃ ZnCo _{0.7} -550/NF	1.65	1.0 M KOH	28
Ni@NC-800/NF	1.60	1.0 M KOH	29

References

- 1 L. Yan, L. Cao, P. Dai, X. Gu, D. Liu, L. Li, Y. Wang and X. Zhao, *Adv. Funct. Mater.*, 2017, **27**, 1703455.
- 2 T. Zhang, J. Du, P. Xi and C. Xu, *ACS Appl. Mater. Interfaces*, 2017, **9**, 362-370.
- 3 J. Yang, G. Zhu, Y. Liu, J. Xia, Z. Ji, X. Shen and S. Wu, *Adv. Funct. Mater.*, 2016, **26**, 4712-4721.
- 4 Z. Yin, C. Zhu, C. Li, S. Zhang, X. Zhang and Y. Chen, *Nanoscale*, 2016, **8**, 19129-19138.
- 5 L. A. Stern, L. Feng, F. Song and X. Hu, *Energy Environ. Sci.*, 2015, **8**, 2347-2351.
- 6 X.-Y. Yu, Y. Feng, B. Guan, X. W. Lou and U. Paik, *Energy Environ. Sci.*, 2016, **9**, 1246-1250.
- 7 L.-A. Stern, L. Feng, F. Song and X. Hu, *Energy Environ. Sci.*, 2015, **8**, 2347-2351.
- 8 B. You, N. Jiang, M. Sheng, M. W. Bhushan and Y. Sun, *ACS Catal.*, 2016, **6**, 714-721.
- 9 M. Wang, M. Lin, J. Li, L. Huang, Z. Zhuang, C. Lin, L. Zhou and L. Mai, *Chem. Commun.*, 2017, **53**, 8372-8375.
- 10 P. W. Menezes, A. Indra, C. Das, C. Walter, C. Göbel, V. Gutkin, D. Schmeißer and M. Driess, *ACS Catal.*, 2016, **7**, 103-109.
- 11 C.-Z. Yuan, S.-L. Zhong, Y.-F. Jiang, Z. K. Yang, Z.-W. Zhao, S.-J. Zhao, N. Jiang and A.-W. Xu, *J. Mater. Chem. A*, 2017, **5**, 10561-10566.
- 12 M. Liu and J. Li, *ACS Appl. Mater. Interfaces*, 2016, **8**, 2158-2165.
- 13 B. You, N. Jiang, M. Sheng, S. Gul, J. Yano and Y. Sun, *Chem. Mater.*, 2015, **27**, 7636-7642.
- 14 J. Song, C. Zhu, B. Z. Xu, S. Fu, M. H. Engelhard, R. Ye, D. Du, S. P. Beckman and Y. Lin, *Adv. Energy Mater.*, 2016, **7**, 1601555.
- 15 J. Li, M. Yan, X. Zhou, Z.-Q. Huang, Z. Xia, C.-R. Chang, Y. Ma and Y. Qu, *Adv. Funct. Mater.*, 2016, **26**, 6785-6796.
- 16 J. Yu, Q. Li, Y. Li, C.-Y. Xu, L. Zhen, V. P. Dravid and J. Wu, *Adv. Funct. Mater.*, 2016, **26**, 7644-7651.
- 17 C. Wang, J. Jiang, T. Ding, G. Chen, W. Xu and Q. Yang, *Adv. Mater. Interfaces*, 2016, **3**.
- 18 H. F. Liang, A. N. Gandi, D. H. Anjum, X. B. Wang, U. Schwingenschlogl and H. N. Alshareef, *Nano Lett.*, 2016, **16**, 7718-7725.
- 19 P. He, X. Y. Yu and X. W. D. Lou, *Angew. Chem., Int. Ed.*, 2017, **56**, 3897-3900.
- 20 M. Ledendecker, S. Krick Calderón, C. Papp, H. P. Steinrück, M. Antonietti and M. Shalom, *Angew. Chem.*, 2015, **127**, 12538-12542.
- 21 J. Tian, Q. Liu, A. M. Asiri and X. Sun, *J. Am. Chem. Soc.*, 2014, **136**, 7587-7590.
- 22 X. Wang, W. Li, D. Xiong and L. Liu, *J. Mater. Chem. A*, 2016, **4**, 5639-5646.
- 23 X. Wang, W. Li, D. Xiong, D. Y. Petrovykh and L. Liu, *Adv. Funct. Mater.*, 2016, **26**, 4067-4077.
- 24 L. Jiao, Y.-X. Zhou and H.-L. Jiang, *Chem. Sci.*, 2016, **7**, 1690-1695.

- 25 N. Jiang, B. You, M. Sheng and Y. Sun, *Angew. Chem.*, 2015, **127**, 6349-6352.
- 26 S. H. Ahn and A. Manthiram, *J. Mater. Chem. A*, 2017, **5**, 2496-2503.
- 27 X. Gao, H. Zhang, Q. Li, X. Yu, Z. Hong, X. Zhang, C. Liang and Z. Lin, *Angew. Chem., Int. Ed.*, 2016, **55**, 6290-6294.
- 28 Y. Wang, W. Wu, Y. Rao, Z. Li, N. Tsubaki and M. Wu, *J. Mater. Chem. A*, 2017, **5**, 6170-6177.
- 29 Y. Xu, W. Tu, B. Zhang, S. Yin, Y. Huang, M. Kraft and R. Xu, *Adv. Mater.*, 2017, **29**.